Published March 14, 2019

Original Research

Core Ideas

- Matric potential controls the equilibrium fractionation factor between soil water and water vapor.
- Surface chemistry determined by X-ray spectroscopy affects the equilibrium fractionation factor.
- A conceptual isotope retention characteristic approach is presented.

The Role of Matric Potential, Solid Interfacial Chemistry, and Wettability on Isotopic Equilibrium Fractionation

Marcel Gaj,* Axel Lamparter, Susanne K. Woche, Jörg Bachmann, Jeffrey J. McDonnell, and C. Florian Stange

Soil water stable isotopes are widely used for geo- and ecohydrological applications. However, the signature of the soil water isotopic composition in the environment depends on various factors. While recent work has shown matric potential effects on equilibrium fractionation, little work has examined other soil parameters concerning soil water energy status like the surface wettability, usually quantified in terms of contact angle. We simultaneously explored the role of matric potential, contact angle, and soil surface chemistry effects on the equilibrium fractionation factor during soil water evaporation. We present a simple laboratory experiment with four different soils of various textures. Subsamples of each texture class were treated with dichlorodimethylsilane to modify surface wetting properties. Additionally, we tested two natural soil samples to explore wettability effects. Samples were dried at temperatures between 40 and 550°C to produce chemically modified surface properties. All samples were spiked with water of known isotopic composition at different water contents. The isotopic signature was determined using the vapor-bag equilibration method. The matric potential of each sample was measured with a soil water potential meter, the contact angle was determined with the sessile drop method, and the surface chemistry by X-ray photoelectron spectroscopy. In addition to temperature and soil matric potential, the elemental composition has apparently some control on the equilibrium fractionation factor. Based on findings, we introduce a new soil water isotope retention characteristic approach to summarize how these factors (matric potential, contact angle, and soil surface chemistry) each control the equilibrium fractionation factor for $^{18}O/^{16}O$ and $^{2}H/H$. Corresponding retention curve approach parameters are promising to be applied in the future to predict soil water fractionation effects under natural and non-stationary conditions.

Abbreviations: CA, contact angle; DCDMS, dichlorodimethylsilane; GMWL, global meteoric water line; IRC, isotope retention characteristic; LEL, local evaporation line; WRC, water retention characteristic.

M. Gaj and J.J. McDonnell, Global Institute for Water Security, School of Environment and Sustainability, Univ. of Saskatchewan, SK S7N 3H5, Canada; M. Gaj, A. Lamparter, and C.F. Stange, Federal Institute for Geosciences and Natural Resources, Soil as a Resource—Properties and Dynamics, D-30655 Hannover, Germany; S.K. Woche and J. Bachmann, Leibniz Univ., Institute of Soil Science, 30419 Hannover, Germany; J.J. McDonnell, School of Geography, Earth & Environmental Sciences, Univ. of Birmingham, Birmingham B15 2TT, UK, and School of Environmental Science and Engineering, South Univ. of Science and Technology of China, Shenzhen, Guangdong 518055, China. *Corresponding author (marcel.gaj@bgr.de).

Received 18 Apr. 2018.
Accepted 23 July 2018.

Citation: Gaj, M., A. Lamparter, S.K. Woche, J. Bachmann, J.J. McDonnell, and C.F. Stange. 2019. The role of matric potential, solid interfacial chemistry, and wettability on isotopic equilibrium fractionation. Vadose Zone J. 18:180083. doi:10.2136/vzj2018.04.0083

The storage and mixing of water in the unsaturated zone is dominated by various processes that interact with physical, chemical, and biological properties of the soil (Vereecken et al., 2016; Pronk et al., 2017). In this context, stable isotopes are a powerful tool to investigate water and water vapor exchange processes between the soil and atmosphere (Dawson et al., 2002), for instance, to trace hydrological processes of terrestrial ecosystems, including subsurface flow pathways (Garvelmann et al., 2012; Stumpp and Maloszewski, 2010; Mueller et al., 2014; Oshun et al., 2016), travel times (Klaus et al., 2015; Sprenger et al., 2016), groundwater recharge (Koeniger et al., 2016), evapotranspiration (Dubbert et al., 2013; Gaj et al., 2016), plant root water uptake (Vargas et al., 2017; Rothfuss and Javaux, 2017) and the partitioning of the global terrestrial water cycle (Evaristo et al., 2015; Good et al., 2015; Bowen, 2015; McDonnell, 2014).

Stable Isotope Fractionation Theory

The isotopic signature of precipitation is depleted in ^{18}O and ^{2}H under cold environmental conditions and enriched under warm environmental conditions. This results in seasonal differences and is reflected in the slope of the global meteoric water line

(GMWL), considering the earth to be a closed system (Craig and Gordon, 1965; Clark and Fritz, 1997). The different vapor pressures of $H_2{}^{18}O$ and $^2H^1H^{16}O$ in equilibrium with the water vapor pressure result in an enrichment of ^2H in the water phase, which is eight times greater than correspondingly for the ^{18}O isotope. In addition to equilibrium fractionation, evaporation entails further kinetic fractionation effects depending on surface temperature, wind speed, and relative humidity. At low or zero relative humidity (~0%), the isotopic enrichment follows a Rayleigh distillation, which means that the isotopic signature of the evaporating water can be simply described by the Rayleigh equation. However, under atmospheric conditions, humidity will mostly be >0%. Then additional fractionation is caused by kinetic effects due to the different diffusivities of $H_2{}^{16}O$, $DH^{16}O$ and $H_2{}^{18}O$ (Clark and Fritz, 1997; Horita et al., 2008) in the liquid and gas phases. During the evaporation process, water vapor diffuses through a transition zone from a boundary layer above the water surface into the atmosphere and vice versa. This is codified in the well-known Craig and Gordon model (Craig and Gordon, 1965). The combined equilibrium and kinetic fractionation effects result in local evaporation lines (LEL) of water from open water bodies with slopes lower than the GMWL (Gat, 2000). The slopes of evaporation lines of open water bodies are related to different environmental conditions such as the relative humidity and can be determined using the stable isotope signatures of the water (Gonfiantini, 1986; Skrzypek et al., 2015). Tracing soil water infiltration and groundwater recharge can be done by simply tracking the time series of the precipitation isotope signature, and mixing, lagging, and damping can be used to estimate travel times through the soil profile (McGuire and McDonnell, 2006). Also, labeling experiments can be used to track soil water movement and water uptake as summarized in recent reviews (Koeniger et al., 2016; Sprenger et al., 2016)

Theory for Isotope Fractionation for Subsurface Water

Compared with the theory applied for stable isotope surface hydrology, the theory for isotope fractionation of subsurface water is more complex. Evaporation from the soil profile as traced by stable isotopes is affected additionally by soil physical properties. An early benchmark presented theoretical and analytical approaches (Barnes and Allison, 1983) to calculate steady state in isothermal and non-steady-state/non-isothermal soil profiles (Barnes and Allison, 1984). These researchers further showed experimentally that the slope of the LEL is controlled by the diffusivity of the water vapor, the tortuosity of the soil pore system, and the evaporation rate (Barnes and Allison, 1988). These experiments were re-examined with subsequent numerical studies (Braud et al., 2009a, 2009b; Rothfuss et al., 2012) and later with higher temporal resolution using in situ approaches (Rothfuss et al., 2015). Model results suggested that the kinetic fractionation factor is associated with the highest uncertainty, especially at the dry end of the water retention curve at low relative humidity. For wet soil, the relative humidity in the pore space is a function of temperature and the energy status of the pore water. Decreasing soil moisture increases the matric potential, i.e., the pressure difference from atmospheric pressure, and reduces the relative humidity in the pore space (Fig. 1).

Methods to determine the isotopic signature from immobile soil water in comparison to bulk water can be difficult and can bias the isotopic signature of the soil water depending on the soil water content (Wassenaar et al., 2008; Hendry et al., 2015), the texture (Orlowski et al., 2016; Koeniger et al., 2011; West et al., 2006), i.e., effects of hydrated cations in the interlayer space of clay minerals (Oerter et al., 2014; Gaj et al., 2017a, 2017b), and the presence of soil carbonate (Meißner et al., 2014). Available methods to determine soil water isotopic signatures

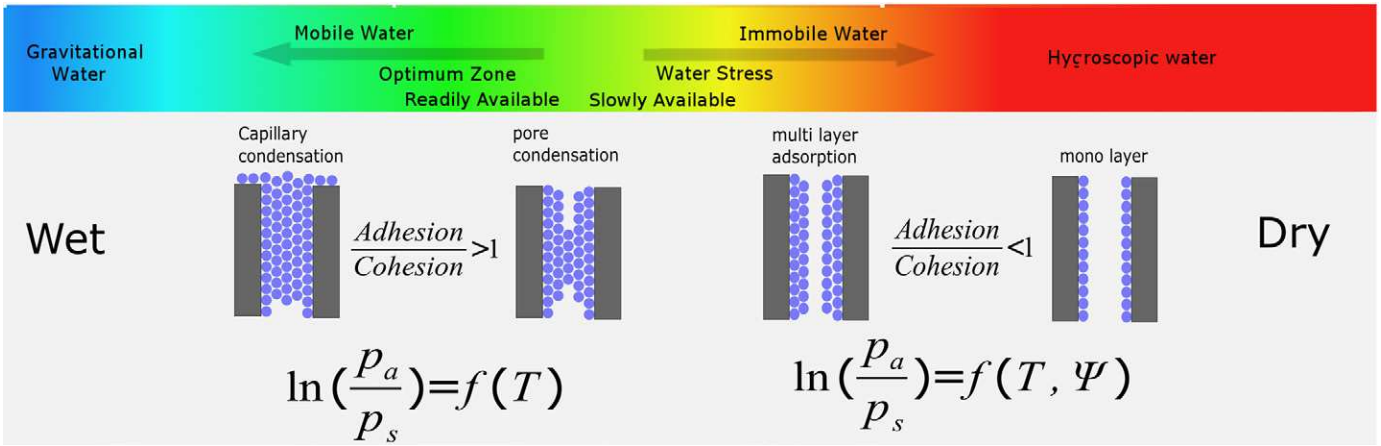

Fig. 1. Different water types such as mobile, immobile and hygroscopic water represented by different color coding. If soils are saturated, water is moved by gravitation (blue). Availability of water for plant-root water uptake has its optimum at or around field capacity (green). During evaporation, a liquid network connects the soil water with the atmosphere. The dominant control on vapor pressure within the pore system is the soil temperature and the pore size. These two variables also define the threshold at which pore condensation occurs. If water is slowly available, then plants have water stress (orange). This is when the water within the pore system forms only thin water films on the soil particle surface. In this situation, the influence of adhesion between the soil particle and the water controls the vapor pressure in addition to temperature. Liquid water transport occurs only via film flow. Water vapor diffuses through the soil profile driven by a vapor pressure gradient.

have been reviewed and theoretically discussed (Sprenger et al., 2015). In an extensive laboratory study, some of these methods were compared using spiked water isotope experiments (Orlowski et al., 2016). It was found that methods that do not require a phase change (i.e., squeezing and centrifugation) did best in recovering the isotopic signature of the spiked water. However, the direct vapor equilibration method (Wassenaar et al., 2008; Hendry et al., 2015) has strong potential for future application because portable laser spectrometers allow vapor sampling in situ (Rothfuss et al., 2013; Volkmann and Weiler, 2014; Gaj et al., 2016; Oerter and Bowen, 2017). This will increase the spatial and temporal resolution of isotope data, reflecting the heterogeneity of water and water vapor fluxes. The time required to reach isotopic equilibrium between soil water and water vapor can vary from minutes in sandy soil, as shown in a field application (Gaj et al., 2016) and for a column experiment in the laboratory (Rothfuss et al., 2015). Depending on the texture of the soil sample equilibrium can also take a few hours to several days after destructive sampling, using the vapor bag equilibration method (Wassenaar et al., 2008; Garvelmann et al., 2012; Hendry et al., 2015; Sprenger et al., 2015). Direct equilibration methods assume that the equilibrium fractionation factor is a function of temperature, as it is for open water surfaces (Majoube, 1971; Wassenaar et al., 2008). Also, other stable isotope related model assumptions such as Rayleigh distillation (Clark and Fritz, 1997), the Craig and Gordon model (Craig and Gordon, 1965), or the non-steady-state leaf water isotope model (Dongmann et al., 1974) require the equilibrium fractionation factor for their application. It has been discussed that relative humidity might control the kinetic fractionation factor (Soderberg et al., 2012). Adsorption experiments showed that the equilibrium fractionation factor is controlled by the vapor pressure (Lin and Horita, 2016; Lin et al., 2018). Other recent work has shown that the equilibrium fractionation factor of natural soil samples is controlled by the matric potential, which, in turn, controls the water vapor pressure (Gaj and McDonnell, 2019).

So, what is the way forward? We know that the physical properties of soils are linked to the pore size distribution, which is affected by soil texture, soil bulk density, as well as the organic matter content (Fig. 1). Water retention characteristics are parameterized in well-known water retention models and their derivatives (Brooks and Corey, 1964; van Genuchten, 1980; Othmer et al., 1991; Peters et al., 2015). In some soils, water retention characteristics are further altered significantly by specific interfacial properties of the particles because the formation of biogeochemical interfaces may produce, in some soils, water-repellent pore surfaces (Bachmann and van der Ploeg, 2002). These changes in wettability also change the shape of the water retention curve to a virtually coarser texture (Bisdom et al., 1993; Bauters et al., 2000; Reszkowska et al., 2014; Liu et al., 2012). Wettability properties can also change with time depending on moisture conditions and the composition of the biogeochemical interface (de Jonge et al., 2007). As illustrated in Fig. 2 (left), the capillary pressure of the liquid phase, which is basically the pressure difference above a curved water meniscus and the pressure inside the meniscus, is also related to the contact angle (CA) that forms at the three-phase boundary of the unsaturated solid–liquid–gas system (Bachmann et al., 2007; Bauters et al., 2000). In this respect, the type of adsorbed cation has been found to be insignificant for wetting properties (Diehl et al., 2014). However, the abundance of cations and their effect on soil organic matter interfacial properties is physically and chemically not yet fully understood (Pronk et al., 2017). Recently it was found for numerous soils that there is a significant relationship

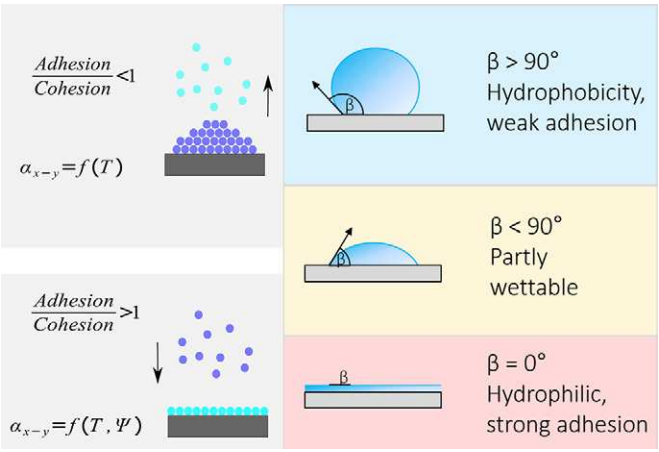

Fig. 2. A water drop on a plane surface develops a particular contact angle β depending on the solid's surface properties (left). An increasing contact angle (CA) causes the surface to be hydrophobic. A hydrophilic soil (CA = 0°), given a particular pore size distribution and water content, shows a higher soil water tension (or lower matric potential) than the same soil with reduced wettability (CA > 0°). The cohesion between water molecules dominates under hydrophobic conditions, and the vapor pressure in the pore system and the equilibrium fractionation factor α are both controlled by the soil temperature. In contrast, a hydrophilic surface causes adhesion between the soil particle surface and the water to control the vapor pressure and α. The unsaturated pore system consists of three phases, the soil particle (solid), the liquid water, and the water vapor (right). Soil particles in a natural system have a coating of particular physio-biogeochemical composition. Artificial hydrophilization was created by treatment with dichlorodimethylsilane (DCDMS). Contact with water (the atmospheric humidity is sufficient) causes hydrolysis of the Cl atoms that are intermediary replaced by hydroxyl groups that form H bonds with surface hydroxyl (silanol) groups. The hydrolyzed Cl atoms react with H atoms to form HCl gas that will evaporate or be dissolved in soil water. Soil water within the air-dry samples may favor HCl formation, possibly causing a drop in pH of the soil solution. Subsequent condensation results in a covalently bonded dimethyl siloxane (DMS) coating of the treated samples, with the two methyl groups pointing toward pore space, thus rendering the surface hydrophobic (Goebel et al., 2013; Hassan et al., 2014). Addition of different amounts of DCDMS varied the degree of reduction in wettability (Bachmann and McHale, 2009). Hydrolyzed DCDMS units not involved in the reaction with the particle surfaces will polymerize to form polydimethylsiloxane (PDMS) that may locate as water-repellent particular bodies between the grains and may additionally affect the CA. Heat treatment with 40, 105, and 550°C affects the coating of the soil particle and creates different surface properties, which has a strong effect on the wettability (Dekker and Ritsema, 1994; Reszkowska et al., 2014; Diehl et al., 2014).

between the wettability (expressed in the CA) and the surface C/O ratio (Woche et al., 2017). However, the link between the wettability in a solid–liquid–gas system and its effect on isotopic fractionation has not yet been examined. Therefore, the objective of the present study was to investigate the relative effects of matric potential, wettability, and soil surface chemistry are the soil water isotopic equilibrium fractionation factor?

Methods

To answer this question, we analyzed soil samples of different textures and samples with similar textures but with different surface properties to cover (i) a wide range of textures, but not swelling–shrinking, (ii) differences in wettability (moderate temperature treatment), (iii) differences in interfacial chemistry (salinization, 550°C treatment), and (iv) model soils vs. natural soils to increase the complexity of the interface.

Sample Description

The schematic of the sample preparation procedure is illustrated and explained in Fig. 2 (right). Soil samples with different textures (see Table 1) were artificially hydrophobized by treatment with dichlorodimethylsilane (DCDMS) (Goebel et al., 2013; Hassan et al., 2014). An additional set of samples was collected from an agricultural field and a nearby (~20 m) coniferous forest (*Pinus sylvestris* L.). The two samples with the same texture but different wettability properties were split into three subsamples. The subsamples were temperature treated (dried for 24 h at 40, 105, or 550°C) to create different surface properties. All samples were subsequently analyzed for texture, surface elemental composition, contact angle, and specific surface area or Brunauer–Emmett–Teller (BET).

Isotope Measurements

The well-known direct equilibration approach was used to determine the stable isotope signatures of the soil water (Wassenaar et al., 2008). This method assumes that soil water quickly reaches thermodynamic equilibrium with the vapor in the head space. Then the bag head space (i.e., the vapor) was measured with a water vapor isotope analyzer (Los Gatos Research, IWA-35-EP). Isotope signatures are reported in δ notation. The δ refers to the measured isotope ratios of the sample, R_{sample}, to an international or laboratory reference standard, $R_{reference}$:

$$\delta = \left(\frac{R_{sample}}{R_{reference}} - 1 \right) \quad [1]$$

The isotope ratio R is defined as the quotient of $N(^{i}\mathrm{E})_P$ and $N(^{j}\mathrm{E})_P$, with the number of each isotope ^{i}E and ^{j}E of chemical element E in substance P expressed as (Coplen, 2011)

$$\mathrm{R}\left(\frac{^{i}\mathrm{E}}{^{j}\mathrm{E}} \right) = \frac{N(^{i}\mathrm{E})_P}{N(^{j}\mathrm{E})_P} \quad [2]$$

Table 1. The names of the samples are given according to the German DIN standards for soil texture classifications. Particle size analysis, total organic C (TOC), total inorganic C (TIC), and applied dichlorodimethylsilane (DCDMS) amount and surface area determined by BET analysis are summarized. One set of samples was artificially hydrophobized using DCDMS as indicated. Samples from an agricultural field (acre) and a forest with similar grain size but different wettability were treated at 40, 105, and 550°C to alter surface properties.

Sample	Particle size distribution			DCDMS	TOC	TIC	Surface area	Slope of the EL†	R^2	p value
	<63 μm	63–630 μm	630–2000 μm							
	%			μL/kg	%		m^2/g			
SS	0	2.5	97.1	–	0.21 ± 0.01	0	0.15	3.03	0.97	<0.0001
SS_5	–	0	–	50			0.11	3.07	0.71	0.0012
Ut2_5	0	11.8	88.2	50	0.01 ± 0	0	0.08	3.78	0.52	0.0052
Ut2_20	0	11.1	88.9	200			0.27	5.47	0.9	0.0001
Ut3	11.7	88.3	0.0	–	0.05 ± 0.01	1.16 ± 0.02	1.09	1.3	0.01	0.7251
Ut3_20	13.3	86.7	0.0	200			0.99	3.03	0.68	0.023
Ut3_60	13.2	86.8	0.0	600			0.81	3.65	0.87	<0.0001
Su1	4.88	17.4	77.7	4000	0.56 ± 0.2	0	26.89	1.19	0.71	0.034
St3	24.11	3.9	72.0	16,000			33.02	1.3	0.98	<0.0001
SS_acre 40	0	7.9	92.1	–	2.06 ± 0.15	0.23 ± 0.01	0.11	7.75	0.85	0.0001
SS_forest 40	0	7.9	92.0	–	2.97 ± 0.24	0.01 ± 0.01	0.20	9.29	0.84	<0.0001
SS_acre 105	0	5.6	94.3	–	1.70 ± 0.03	0.28 ± 0.03	0.12	1.94	0.52	<0.0002
SS_forest 105	0	6.6	93.4	–	2.77 ± 0.44	0.02 ± 0.01	0.02	2.46	0.22	<0.0329
SS_acre 550	0	4.2	95.7	–	0.02 ± 0.0	0.21 ± 0.04	0.57	4.71	0.65	<0.0001
SS_forest 550	0	3.5	96.5	–	0.01 ± 0.0	0	0.40	4.13	0.5	0.0011

† EL, evaporation line.

The laboratory standards had δ values of 200.4 and −26.2‰ for the enriched and 3.0 and −0.1‰ for the depleted standard for ^{2}H and ^{18}O, respectively. All samples were normalized with a two-point calibration using the laboratory standards. The laboratory standards were calibrated to the international reference scale Vienna Standard Mean Ocean Water–Standard Light Antarctic Precipitation (VSMOWSLAP).

We calculated our tension-based fractionation factor $\alpha^{i/j}E_{p/Q}$ based on the isotope ratio of the labeled water $R(^{i}E/^{j}E)_{Q}$ and the isotope ratio of the measured water vapor $R(^{i}E/^{j}E)_{P}$ as follows:

$$\alpha^{i/j}E_{P/Q}=\frac{R(^{i}E/^{j}E)_{P}}{R(^{i}E/^{j}E)_{Q}}=\frac{1000+\delta_{P}}{1000+\delta_{Q}}=a_{x-y} \quad [3]$$

where a_{x-y} is used as simplified notation for the equilibrium fractionation factor.

Sample Preparation and Measurement Procedure

All DCDMS-treated soil samples and their untreated controls (each 100 g) were oven dried at 105°C for 24 h and subsequently labeled with deionized water of known isotopic signature. Soil water contents in the range from 0.1 to 6% of the weight of the soil sample were prepared in individual Ziploc bags.

To preserve the surface properties achieved by drying at specific temperatures, the two soil samples had been spiked after thermal treatment for 24 h at 40 and 105°C. The samples treated with 550°C were also again dried at 105°C prior to the spiking. All samples were cooled down to room temperature after placing them into a desiccator. In contrast to the DCDMS-treated sample set, the headspace measurements were done 1, 24, and 72 h after adding the spiked water to the 200-g soil sample. After each headspace measurement, a subsample was measured for soil tension with the WP4 water potential meter as explained below. Bags were immediately sealed after subsamples were taken out. The headspace was not refilled with dry air to avoid evaporation effects. Instead, the vapor of the headspace was circulated through the laser spectrometer. After inserting a needle into the Ziploc bag, headspace gas from the bag was extracted into the instrument. When the measured mixing ratio approached its maximum, a second needle was inserted into the bag. This second needle returned the exhaust flow of the analyzer into the bag. In that way, the gas was circulated between the analyzer and the bag. The bags and the transport lines had the same temperature. Hence there was no condensation during the sampling procedure (isothermal conditions). All standards were measured in the same way. A quality check standard was measured with each sequence, using water of known isotopic composition treated the same as the samples. After normalization of the data, the known value of the quality check was compared with the measured value. The difference between the two was 0.4‰ for $\delta^{18}O$ values and 2.32‰ for $\delta^{2}H$ values. This is by definition the trueness of the measurement procedure (Barwick and Prichard, 2011).

To account for the water loss by evaporation into the headspace of the sample bags, the theoretical new equilibrium fractionation factor was calculated according to Gat et al. (1994):

$$R_{f}=\frac{R_{0}}{\alpha-f(\alpha-1)} \quad [4]$$

where R_0 is the initial isotope ratio and R_f is the isotope ratio of the remaining fraction f. According to Eq. [4], the mean enrichment due to a water loss into the headspace was 0.14‰ for $\delta^{18}O$ values and 1.15‰ for $\delta^{2}H$ values. Water amount effects are therefore camouflaged by the accuracy of our bag method as determined from the quality check. Further, mixing ratio dependencies of the laser spectrometer were considered and were insignificant within the range we measured.

Soil Tension Measurements

Matric potential was measured on a WP4C water potential meter (Decagon Devices). This psychrometer device has a precision of ±0.1MPa between 0 and −10 MPa and ±1% between −10 and −300 MPa (Gubiani et al., 2013). The water potential meter measures the combined osmotic (ψ_{os}) and matric potentials (ψ_{m}). The osmotic potential was determined from the electrical conductivity (EC) of the soil solution after adding 50 mL of deionized water to 100 g of soil sample. Then ψ_{os} can be calculated as recommended in the manual of the WP4:

$$\psi_{os}=-0.036EC\left(\frac{\theta_{s}}{\theta}\right) \quad [5]$$

where EC (dS/m) is the electrical conductivity of the solution, θ_s (g/g) is the water content at saturation, and θ (g/g) is the actual water content. Then water retention curves were plotted from the known gravimetric water content and the calculated matric potential (combined potential minus osmotic potential).

X-ray Photoelectron Spectroscopy

The surface elemental composition of the thermally treated natural soils was determined with X-ray photoelectron spectroscopy (maximum analysis depth 10 nm). Survey spectra were recorded with an Axis Ultra DLD device (Kratos Analytical), using Al Kα radiation (1486.7 eV) at 20 mA, 12 kV, and with a pass energy of 160 eV. Spectra were quantified with the software Vision 2 (Kratos Analytical), using the implemented relative sensitivity factors.

Contact Angle

The CA was determined with the sessile drop method using a CCD-equipped CA microscope (OCA 15, Data Physics). The material was fixed on a microscope slide with double-sided adhesive tape as a single-grain layer, and the placement of a drop (1 mL) of water was recorded. The initial CA was evaluated directly after placement of the drop and at the end of mechanical disturbances by drop shape analysis (ellipsoidal fit) and fit of tangents on the left and the right sides (Goebel et al., 2013). The CA is given as the mean of six drops (n = 12).

Results

Dichlorodimethylsilane Treatment Effects

The CA increased with an increasing amount of the applied DCDMS. The texture of most samples remained unaffected by the DCDMS treatment (Table 1). There was one exception: clay sample C1, which had been treated with the highest amount of DCDMS, showed an increase in the clay fraction in conjunction with an increase in the specific surface area. The DCDMS treatment increased the specific surface area for the fine sand about 30% (Ut2), but decreased the specific surface area for the silt sample by 30% (Ut3) and also increased the clayey sample (Su1/St3) by 20%. A comparison of the CA measurement before and after the vapor bag experimental procedure for isotope sampling confirmed the stability of the coating for the field sand samples (values within the uncertainty of the measurement, see Table 2). An additional increase in CA after the vapor bag experimental procedure was observed for the silt samples. However, hydrophobicity created by the DCDMS treatment of the clay samples decreased after the entire experimental procedure (drying, rewetting, isotope sampling, and water potential measurement). The DCDMS treatment of the clay samples resulted in an initial CA of 51°, and 105° directly after treatment. After drying at 105°C, rewetting, and isotope sampling, the initial CA of the clay sample treated with 4000 μL DCDMS/kg (400 μL per 100 g) was reduced to from 51 to 18°, while the CA of the other clay sample (16,000 μL DCDMS/kg or 1600 μL per 100 g) was reduced by 39 to 66°.

Thermal Treatment Effects

The texture of the natural samples remained unaffected by the heat treatment (Table 1). Thermal treatment with 550°C decolorized the samples due to the removal of organic compounds, increased the specific surface area, and resulted in complete wettability, i.e., CA = 0°. Removal of the coating caused an increase in the content of the mineral-derived cations (especially Si, Al, and Ca) and O and a decrease of C and N content within the X-ray photoelectron spectroscopy analysis depth (Table 3). The surface O/C ratio increased in accordance with an increase in wettability, i.e., decrease in the CA (Woche et al., 2017). While N was absent in the interface after thermal treatment at 550°C, the C content still was up to 20 atom%, probably due to adventitious C, i.e., C compounds adsorbed to the particle surfaces from the surrounding air. Thermal treatment of the natural soil material at 105°C resulted in an increase in C and a decrease in O content. The surface O/C ratio accordingly decreased after 105°C treatment and CA increased. The specific surface area of the forest samples increased with increasing temperature, while samples from the agricultural site did not show an effect of the thermal treatment on the specific surface area (Table 2). Effects of the temperature treatment on the water retention characteristic (WRC) and the equilibrium fractionation factor are depicted in Fig. 3.

Water Retention Characteristic

The shape of the WRC of the DCDMS-treated soil samples did not change compared with the untreated control. Samples dried at 40 and 105°C that also had a change in CA showed similar moisture release curves in the measured low-moisture range between pF > 3 and pF < 6, like the silane-treated samples. The highest matric potential values were observed above pF 5.5 (31.6 MPa) at 0.05 kg/kg water content. In contrast, samples dried at 550°C reached a maximum soil tension of pF 4.5 (3.16 MPa). The most scatter of water content was observed between the different time steps at or below the wilting point, as indicated by the error bars (Fig. 3). A change toward higher soil tension with time was most pronounced for the samples dried at 40°C. Only small variations in water content were observed for the samples dried at 105 and 550°C.

Table 2. Initial contact angle (CA_ini) and contact angles after 5 s (CA_5s) of the dichlorodimethylsilane (DCDMS)-treated samples determined before (pre) and after (post) determination of the isotope retention characteristic. The volumes given refer to the applied amount of DCDMS.

Sample treatment	CA_ini	CA_5s
	°	
Sample SS		
Original	48.6 (8.5)†	18.7 (16.8)
5 μL_{pre}	83.6 (5.5)	56.0 (5.9)
5 μL_{post}	70.1 (10.1)	62.6 (12.6)
10 μL_{pre}	93.6 (7.3)	81.3 (12.0)
10 μL_{post}	85.6 (10.0)	66.4 (9.3)
Sample Ut2		
$Orig_{pre}$	49.0 (4.1)	37.6 (8.5)
$Orig_{post}$	53.5 (6.1)	31.2 (8.9)
5 μL_{pre}	111.0 (7.0)	96.4 (9.9)
5 μL_{post}	108.2 (4.3)	91.0 (10.7)
20 μL_{pre}	97.9 (4.6)	89.9 (4.2)
20 μL_{post}	91.0 (6.7)	73.3 (5.3)
Sample Ut3		
$Orig_{pre}$	13.7 (4.3)	0.0 (0.0)
$Orig_{post}$	36.8 (6.9)	1.0 (0.0)
20 μL_{pre}	49.2 (7.6)	3.0 (4.9)
20 μL_{post}	73.5 (4.6)	40.7 (4.9)
60 μL_{pre}	60.2 (5.1)	27.8 (7.7)
60 μL_{post}	87.0 (3.3)	63.6 (6.6)
Sample Su1/St3		
400 μL_{pre}	52.6 (9.8)	1.0 (0.0)
400 μL_{post}	18.3 (9.7)	1.0 (0.0)
1600 μL_{pre}	104.5 (9.5)	61.5 (6.0)
1600 μL_{post}	66.3 (13.3)	22.3 (17.2)

† Mean with standard deviation in parentheses (n = 12).

Table 3. Surface chemistry of thermally treated soil samples determined by X-ray photoelectron spectroscopy (XPS) analysis as atomic percentage of elements found. The XPS analyses of the samples were done before (pre) and after (post) determination of the isotope retention characteristic. Additionally, initial contact angles (CA_ini) and contact angles after 5 s (CA_5s) were determined and did not change.

	Na	Fe	O	N	Ca	K	C	Cl	P	Si	Al	Mg	O/C	Si/C	CA_ini	CA_5s
	atom%														°	
SS_acre																
40_{pre}	0.00 (0.00)†	0.22 (0.03)	39.35 (0.68)	2.30 (0.08)	1.07 (0.08)	0.05 (0.06)	47.76 (0.83)	0.05 (0.05)	0.17 (0.12)	6.23 (0.57)	2.62 (0.32)	0.17 (0.18)	0.82 (0.03)	0.13 (0.01)	78.50 (8.41)	37.65 (14.5)
40_{post}	0.00 (0.00)	0.03 (0.03)	40.82 (0.98)	1.44 (0.20)	0.02 (0.02)	0.01 (0.01)	44.50 (0.58)	0.04 (0.05)	0.02 (0.03)	12.38 (0.74)	0.69 (0.25)	0.06 (0.06)	0.92 (0.03)	0.28 (0.02)	102.00 (5.10)	87.66 (11.1)
105_{pre}	0.05 (0.05)	0.05 (0.05)	34.36 (1.74)	2.85 (0.11)	1.07 (0.05)	0.00 (0.01)	54.86 (2.66)	0.02 (0.02)	0.23 (0.10)	4.26 (0.56)	2.11 (0.39)	0.16 (0.07)	0.63 (0.06)	0.08 (0.01)	122.79 (6.80)	116.24 (5.7)
105_{post}	0.00 (0.00)	0.09 (0.03)	33.18 (1.23)	2.66 (0.20)	1.10 (0.07)	0.01 (0.01)	56.24 (2.13)	0.01 (0.01)	0.24 (0.01)	4.19 (0.43)	2.11 (0.38)	0.18 (0.14)	0.59 (0.04)	0.07 (0.01)	122.73 (9.35)	120.07 (10.1)
550_{pre}	0.05 (0.02)	0.51 (0.12)	54.80 (3.76)	0.09 (0.11)	4.35 (0.28)	0.03 (0.02)	20.65 (5.89)	0.00 (0.01)	1.11 (0.06)	11.87 (1.85)	5.93 (0.64)	0.60 (0.31)	2.83 (0.95)	0.62 (0.26)	1.00 (0.00)	0.00 (0.0)
550_{post}	0.00 (0.00)	0.46 (0.12)	56.73 (1.66)	0.03 (0.03)	4.33 (0.54)	0.02 (0.02)	20.29 (3.52)	0.24 (0.08)	0.88 (0.12)	8.30 (0.50)	7.83 (1.25)	0.89 (0.29)	2.86 (0.53)	0.42 (0.06)	1.00 (0.00)	0.00 (0.0)
SS_forest																
40_{pre}	0.01 (0.01)	0.07 (0.07)	36.70 (1.06)	1.52 (0.26)	0.03 (0.01)	0.01 (0.02)	50.83 (2.51)	0.02 (0.01)	0.03 (0.01)	10.27 (1.79)	0.45 (0.09)	0.07 (0.04)	0.72 (0.06)	0.20 (0.04)	105.37 (10.65)	90.36 (11.9)
40_{post}	0.00 (0.01)	0.16 (0.07)	38.28 (0.27)	2.98 (0.09)	1.22 (0.05)	0.01 (0.01)	49.18 (0.76)	0.03 (0.02)	0.27 (0.06)	5.38 (0.60)	2.24 (0.08)	0.25 (0.17)	0.78 (0.02)	0.11 (0.01)	91.40 (7.36)	54.04 (9.7)
105_{pre}	0.00 (0.00)	0.05 (0.05)	33.76 (0.92)	1.27 (0.05)	0.07 (0.03)	0.01 (0.01)	53.96 (1.86)	0.02 (0.02)	0.03 (0.03)	10.07 (0.98)	0.65 (0.09)	0.11 (0.07)	0.63 (0.04)	0.19 (0.02)	129.17 (6.13)	124.01 (9.0)
105_{post}	0.00 (0.01)	0.05 (0.05)	31.22 (2.00)	1.19 (0.12)	0.06 (0.03)	0.00 (0.01)	57.96 (3.73)	0.01 (0.01)	0.02 (0.02)	8.86 (1.56)	0.50 (0.05)	0.13 (0.12)	0.54 (0.07)	0.15 (0.04)	134.50 (15.66)	130.28 (13.8)
550_{pre}	0.14 (0.06)	0.28 (0.12)	59.73 (2.15)	0.03 (0.03)	0.37 (0.04)	0.25 (0.33)	15.00 (4.27)	0.02 (0.02)	0.08 (0.06)	20.33 (2.09)	3.49 (0.15)	0.28 (0.08)	4.25 (1.45)	1.47 (0.58)	1.00 (0.00)	0.00 (0.0)
550_{post}	0.09 (0.02)	0.64 (0.07)	58.44 (2.48)	0.04 (0.04)	0.83 (0.11)	0.15 (0.05)	16.97 (3.74)	0.06 (0.04)	0.24 (0.07)	15.27 (0.78)	7.07 (0.46)	0.19 (0.05)	3.57 (0.83)	0.93 (0.23)	1.00 (0.00)	0.00 (0.0)

† Mean with standard deviation in parentheses.

Isotope Retention Characteristic

The isotope retention characteristic (IRC) can be considered as an analog to the water retention characteristic. Instead of illustrating the relationship between matric potential and water content, the IRC expresses the relationship between the matric potential ψ and the equilibrium fractionation factor between bound water and water vapor (α_{x-y}). The IRC is presented here for soil samples with different grain sizes and different interfacial properties.

The IRCs of the natural soil samples showed an increase of slope with increasing temperature from 40 to 105°C, while the 550°C treated samples were similar to the 40°C samples (Fig. 3). Samples dried at 105°C plotted along the same regression line as found by Gaj and McDonnell, (2019), considering all values below pF 5. Values above pF 5 showed a decrease in α_{x-y} only for the samples dried at 105°C. The equilibrium fractionation factor of samples dried at 40°C steadily increased until pF 6. A less distinct IRC was observed for the samples dried at 550°C. The error bars in Fig. 3 for the agricultural and forest samples indicate the standard deviation of the equilibrium fractionation factor α_{x-y} from the sampling after 1, 24, and 72 h. A mean over the standard deviation for all water contents for $\alpha^{18}O$ values was 0.46×10^{-4} for the sample forest_40, 0.65×10^{-4} for forest_105, and 0.75×10^{-4} for forest_550. These values were higher for the agricultural site samples, with 0.8×10^{-4}, 1.04×10^{-4}, and 1.4×10^{-4} for acre_40, acre_105, and acre_550, respectively. Therefore, the most consistent fractionation factors with respect to a small standard deviation with time were observed for the samples dried at 105°C, indicating more stable and homogenous surface properties. The same standard deviation calculated for $\alpha^{2}H$ values was 4.5×10^{-4} for the sample forest_40, 4.8×10^{-4} for forest_105, and 5×10^{-4} for forest_550. These values were higher for the agricultural samples, with 4.3×10^{-4}, 4.3×10^{-4}, and 4.8×10^{-4} for acre_40, acre_105, and acre_550, respectively.

Dual isotope plots of the temperature-treated soil samples are depicted in Fig. 4. Commonly a LEL derived from soil water isotope signatures relates two vertical distributed variables to each other. The LELs shown here are a result of matric potential effects on the equilibrium fractionation between the bound water and the water vapor. No actual evaporation occurred during the experiment. The slopes of the evaporation lines of the DCDMS-treated silt samples varied between 1 and 6.4 (Table 1); smaller slopes were observed for the clay samples. Dual isotope plots of the natural soil samples grouped according to the applied drying temperature. The slope of the LELs of all natural soil samples changed slightly during the course of 3 d (expressed by the error bars). The greatest slopes (6.6–15.9) were observed for the samples dried at 40°C. The δ values plot parallel to the GMWL. Generally, an increasing CA

can be attributed to higher slopes of the evaporation lines (Fig. 4 and 5) until a CA = 90°. The slope of the evaporation line decreases from 90° to higher CAs. The samples treated at 550°C do not fit into the general picture. Neither the relationship between the contact angle and the O/C ratio nor the relationship between the slope of the evaporation line and the CA aligns with the other samples.

Discussion

Matric Potential, Solid Interfacial Chemistry, and Wettability

A shift in the WRC for water-repellent soil samples toward lower matric potentials—as shown by Lamparter et al. (2014) and Reszkowska et al. (2014)—was not observed in this study for the analyzed soil samples and at the applied water content. Instead, our observations are in agreement with a previous study that showed no or minor effects of the wettability to the WRC at or around the wilting point for hydrophobic and hydrophilic soil samples with similar texture (Liu et al., 2012).

Isotope Retention Characteristic and Wettability

The physical properties controlling the storage and release of water are strongly related to the surface chemical composition and the binding state of the water molecule layers adsorbed to the particle surfaces. A change of the physicochemical structure of organic matter has consequences for the mobility and adsorption of water (Diehl et al., 2014). Sorption of non-polar organic compounds as well as heat treatment has a strong effect on particle wettability (Dekker and Ritsema, 1994; Reszkowska et al., 2014; Diehl et al., 2014; Woche et al., 2017). This has corresponding effects on the spatial distribution of the water content, on the binding state of thin water films on particles surfaces (Churaev, 2000), as well as on the shape and the radius of single water menisci (Müehl et al., 2012). Consequently, this affects the energetic interfacial equilibrium state of the water vapor pressure in a solid–water–vapor system and changes the equilibrium fractionation factor for $^{18}O/^{16}O$ and $^{2}H/^{1}H$. However, as could be shown here, the grain size distribution has the major control on the isotopic equilibrium fractionation factor if non-polar organic compounds are camouflaged by surface hydroxyl groups of silane.

Isotope Retention Characteristic and Surface Chemistry

In contrast, if the wettability is associated with the C/O ratio, the slope of the evaporation line changes correspondingly. Therefore, our data provide evidence that the chemical composition as expressed by the wettability of the particle surfaces affects the equilibrium fractionation factor, i.e., the sessile drop contact angle might control the slope of the evaporation lines without DCDMS (Fig. 5). However, more data are needed to confirm this relationship for both DCDMS-treated and natural soil samples.

Secondary Findings and Future Work

The applicability of the vapor bag equilibration method has been constrained by a lower limit of 3 g of water within the bag (Wassenaar et al., 2008) due to water loss into the headspace that enriches the original isotope signature of the sample. The data

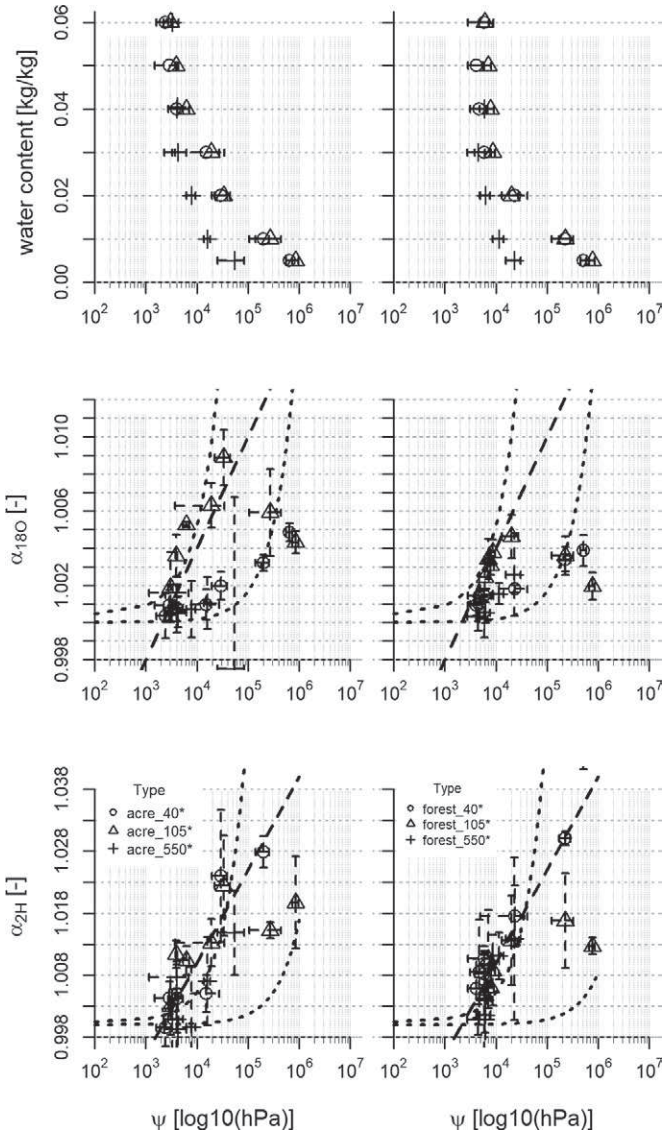

Fig. 3. Water retention characteristics (top row), the equilibrium fractionation factor α for ^{18}O (middle row), and α for ^{2}H (lower row) are shown. Samples from the agricultural field (left) and the forest (right) were treated with 40, 105, and 550°C. The heat treatment with 550°C reduced the matric potential compared with the treatment with lower temperature. Samples from the field have a lower matric potential below the wilting point compared with the forest soil. The equilibration time appeared to have an only minor impact on the moisture release curve and is indicated by the error bars. The α for ^{18}O increases with increasing soil tension (middle row). The dotted lines show the calculated α using the Kelvin equation with a contact angle of 0° (upper curve) and a contact angle of 88° (lower curve). All values plot within the calculated α values using the Kelvin equation. A regression line found by Gaj and McDonnell (2019) is also indicated (dashed gray). Heat treatment of the field samples at 105°C resulted in higher slopes of $\alpha^{18}O$. In contrast, $\alpha^{2}H$ does not show a strong effect on the shape of the isotope retention curve.

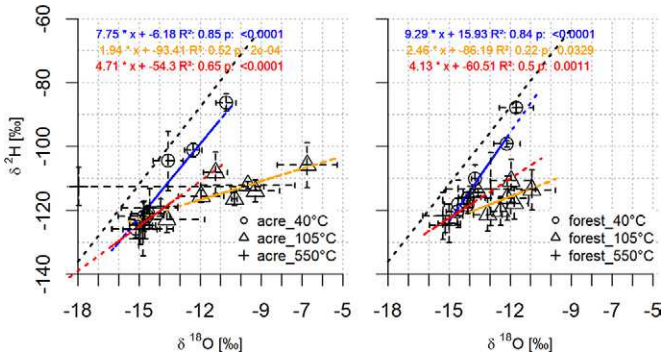

Fig. 4. The global meteoric water line (GMWL, dashed black), the local evaporation lines (LEL), their slope, intercept, and R^2 are indicated in corresponding color coding. The heat treatment altered the wettability of the samples collected from the agricultural field (acre) and the forest. This caused a change of slope in dual isotope space, while all samples have the same grain size. Samples dried at 40°C plot parallel to the GMWL. Heat treatment at 105°C resulted in slopes that are found in arid zones. Drying at 550°C resulted in a slope between the two 40 and 105°C sample sets.

presented here have already conclusively shown that the water content by itself is not the limiting factor to get an unaffected isotopic signature with this method. It is merely the combination of soil tension, the surface chemical composition, and the wettability that controls the equilibrium fractionation between tightly bound or immobile water and water vapor within the pore space. Therefore, the isotopic signature of tightly bound water can be determined with the vapor bag equilibration method if the IRC is known. This approach extends the applicability of direct water vapor equilibration methods and consequently the use of in situ measurements.

As shown here, the drying of soil samples affects the surface properties and the surface properties control the equilibrium fractionation factor. It is critical to develop a method for the determination of the IRC of natural soil samples that does not affect the surface properties. Whether other soil water extraction methods are affected by the surface elemental conditions is not known.

Conclusion

We provide evidence that wettability, grain size distribution, and the surface elemental composition of solids affect the equilibrium fractionation factor in different ways. The primary control on the equilibrium fractionation factor of soil water is the grain size distribution. Second, the wettability (as expressed by the contact angle) of surfaces has an insignificant effect on the equilibrium conditions if the surface elemental composition is camouflaged by DCDMS. However, the wettability controls the slope of the evaporation line if water and water vapor can interact with the surface elemental composition of the soil grain surface. This has been shown by soil samples that were treated at different temperatures.

Therefore, the degree of transport, mixing, and fractionation of water stable isotopes within the unsaturated zone under drought is controlled by the composition of the biogeochemical interface, soil tension, and wettability. Further, the presented data have some important implications from a methodological perspective. Sample preparation using oven-dried samples should consider that surface properties change and that this might affect the isotopic signature of the bound water. Especially the use of stable isotope signatures of soil water and water vapor at the dry end of the water retention curve (around the wilting point) is largely unexplored but nevertheless important, since these dry conditions occur preferentially at the shallow soil depths where evaporation into the atmosphere occurs.

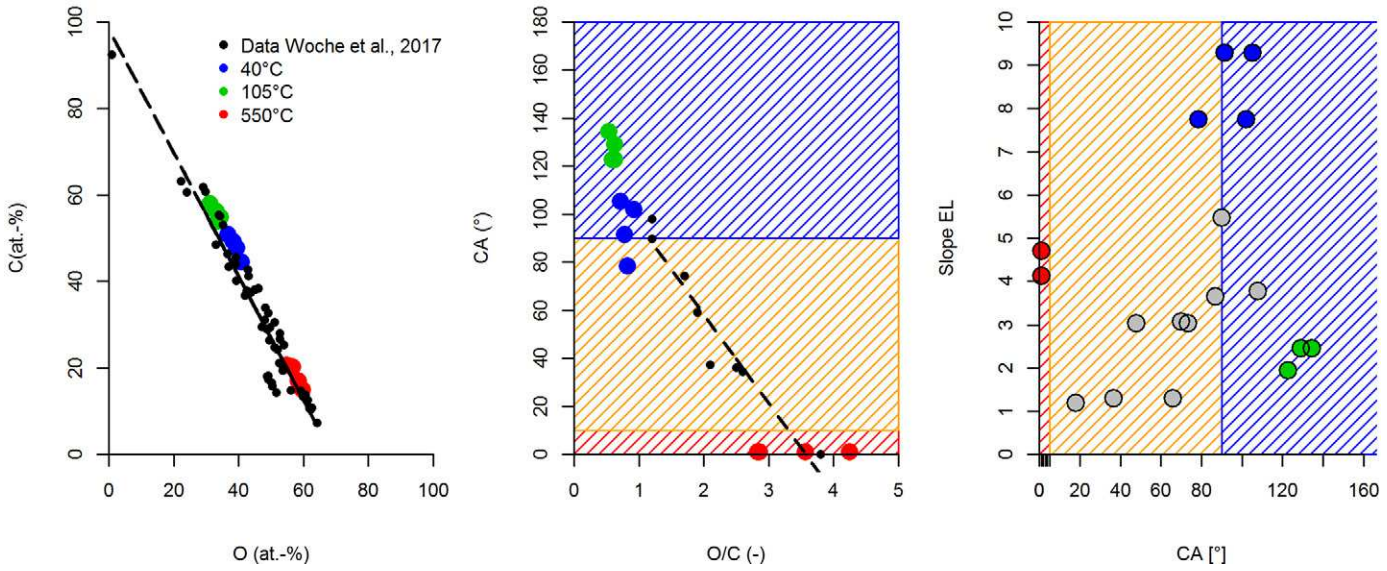

Fig. 5. The relationships between surface O and C (atom%, left), the surface O/C ratio and the contact angle (CA, center), and the CA angle and the slope of the local evaporation line (EL) (right). Samples coated with dichlorodimethylsilane (DCDMS) showed an increasing slope of the EL along with an increasing CA. The heat-treated soils show a decrease of the C/O ratio and an increase of the CA. The slope of the EL increased with increasing CA to 90° and decreased above that threshold. A relationship between the grain size distribution and the slope of the EL could not be found.

These soil layers are also enriched with organic matter, changing the wettability and solid particle interfacial chemistry. Studies using soil water stable isotopes should consider corresponding fractionation effects for better understanding and quantification of using stable water isotopes for environmental studies. Neglecting these effects can bias application of direct equilibration methods and calculations using models that assume constant equilibrium fractionation factors during soil water evaporation.

References

Bachmann, J., M. Deurer, and G. Arye. 2007. Modeling water movement in heterogeneous water-repellent soil: 1. Development of a contact angle-dependent water-retention model. Vadose Zone J. 6:436–445. doi:10.2136/vzj2006.0060

Bachmann, J., and G. McHale. 2009. Superhydrophobic surfaces: A model approach to predict contact angle and surface energy of soil particles. Eur. J. Soil Sci. 60:420–430.

Bachmann, J., and R.R. van der Ploeg. 2002. A review on recent developments in soil water retention theory: Interfacial tension and temperature effects. J. Plant Nutr. 165:468–478. doi:10.1002/1522-2624(200208)165:4<468::AID-JPLN468>3.0.CO;2-G

Barnes, C.J., and G.B. Allison. 1983. The distribution of deuterium and ^{18}O in dry soils: 1. Theory. J. Hydrol. 60:141–156. doi:10.1016/0022-1694(83)90018-5

Barnes, C.J., and G.B. Allison. 1984. The distribution of deuterium and ^{18}O in dry soils: 3. Theory for non-isothermal water movement. J. Hydrol. 74:119–135. doi:10.1016/0022-1694(84)90144-6

Barnes, C.J., and G.B. Allison. 1988. Tracing of water movement in the unsaturated zone using stable isotopes of hydrogen and oxygen. J. Hydrol. 100:143–176. doi:10.1016/0022-1694(88)90184-9

Barwick, V., and E. Prichard. 2011. Terminology in analytical measurement: Introduction to VIM 3. Eurachem, Zug, Switzerland.

Bauters, T.W.J., T.S. Steenhuis, D.A. DiCarlo, J.L. Nieber, L.W. Dekker, C.J. Ritsema, et al. 2000. Physics of water repellent soils. J. Hydrol. 231–232:233–243. doi:10.1016/S0022-1694(00)00197-9

Bisdom, E.B.A., L.W. Dekker, and J.T. Schoute. 1993. Water repellency of sieve fractions from sandy soils and relationships with organic material and soil structure. Geoderma 56:105–118. doi:10.1016/0016-7061(93)90103-R

Braud, I., T. Bariac, P. Biron, and M. Vauclin. 2009a. Isotopic composition of bare soil evaporated water vapor: II. Modeling of RUBIC IV experimental results. J. Hydrol. 369:17–29. doi:10.1016/j.jhydrol.2009.01.038

Braud, I., P. Biron, T. Bariac, P. Richard, L. Canale, J.P. Gaudet, and M. Vauclin. 2009b. Isotopic composition of bare soil evaporated water vapor: I. RUBIC IV experimental setup and results. J. Hydrol. 369:1–16. doi:10.1016/j.jhydrol.2009.01.034

Brooks, R., and T. Corey. 1964. Hydraulic properties of porous media. Hydrol. Pap. 3. Colorado State Univ., Fort Collins.

Bowen, G. 2015. Hydrology: The diversified economics of soil water. Nature 525:43–44. doi:10.1038/525043a

Churaev, N.V. 2000. Liquid and vapour flows in porous bodies: Surface phenomena. Top. Chem. Eng. 13. CRC Press, Boca Raton, FL.

Clark, I.D., and P. Fritz. 1997. Environmental isotopes in hydrogeology. CRC Press, Boca Raton, FL.

Coplen, T.B. 2011. Guidelines and recommended terms for expression of stable-isotope-ratio and gas-ratio measurement results. Rapid Commun. Mass Spectrom. 25:2538–2560. doi:10.1002/rcm.5129

Craig, H., and L.I. Gordon. 1965. Deuterium and oxygen 18 variations in the ocean and the marine atmosphere. In: E. Tongiorgi, editor, Stable isotopes in oceanographic studies and paleotemperatures. Laboratorio di Geologia Nucleare, Pisa, Italy. p. 9–130.

Dawson, T.E., S. Mambelli, A.H. Plamboeck, P.H. Templer, and K.P. Tu. 2002. Stable isotopes in plant ecology. Annu. Rev. Ecol. Syst. 33:507–559. doi:10.1146/annurev.ecolsys.33.020602.095451

de Jonge, L.W., P. Moldrup, and O.H. Jacobson. 2007. Soil-water content dependency of water repellency in soils: Effect of crop type, soil management and physical-chemical parameters. Soil Sci. 172:577–588. doi:10.1097/SS.0b013e318065c090

Dekker, L.W., and C.J. Ritsema. 1994. How water moves in a water repellent sandy soil: 1. Potential and actual water repellency. Water Resour. Res. 30:2507–2517. doi:10.1029/94WR00749

Diehl, D., T. Schneckenburger, J. Krüger, M.-O. Goebel, S.K. Woche, and J. Schwarz. 2014. Effect of multivalent cations, temperature and aging on soil organic matter interfacial properties. Environ. Chem. 11:709–718. doi:10.1071/EN14008

Dongmann, G., H.W. Nürnberg, H. Förstel, and K. Wagener. 1974. On the enrichment of $H_2{}^{18}O$ in the leaves of transpiring plants. Radiat. Environ. Biophys. 11:41–52. doi:10.1007/BF01323099

Dubbert, M., M. Cuntz, A. Piayda, C. Maguás, and C. Werner. 2013. Partitioning evapotranspiration: Testing the Craig and Gordon model with field measurements of oxygen isotope ratios of evaporative fluxes. J. Hydrol. 496:142–153. doi:10.1016/j.jhydrol.2013.05.033

Evaristo, J., S. Jasechko, and J.J. McDonnell. 2015. Global separation of plant transpiration from groundwater and streamflow. Nature 525:91–94. doi:10.1038/nature14983

Gaj, M., M. Beyer, P. Koeniger, H. Wanke, J. Hamutoko, and T. Himmelsbach. 2016. In situ unsaturated zone water stable isotope (^2H and ^{18}O) measurements in semi-arid environments: A soil water balance. Hydrol. Earth Syst. Sci. 20:715–731. doi:10.5194/hess-20-715-2016

Gaj, M., S. Kaufhold, P. Koeniger, M. Beyer, M. Weiler, and T. Himmelsbach. 2017a. Mineral mediated isotope fractionation of soil water. Rapid Commun. Mass Spectrom. 31:269–280. doi:10.1002/rcm.7787

Gaj, M., S. Kaufhold, and J.J. McDonnell. 2017b. Potential limitation of cryogenic vacuum extractions and spiked experiments. Rapid Commun. Mass Spectrom. 31:821–823. doi:10.1002/rcm.7850

Gaj, M., and J.J. McDonnell. 2019. Possible soil tension controls on the isotopic equilibrium fractionation factor for evaporation from soil. Hydrol. Processes. doi:10.1002/hyp.13418

Gat, J.R. 2000. Atmospheric water balance: The isotopic perspective. Hydrol. Processes 14:1357–1369.

Gat, J.R., C.J. Bowser, and C. Kendall. 1994. The contribution of evaporation from the Great Lakes to the continental atmosphere: Estimate based on stable isotope data. Geophys. Res. Lett. 21:557–560. doi:10.1029/94GL00069

Garvelmann, J., C. Külls, and M. Weiler. 2012. A porewater-based stable isotope approach for the investigation of subsurface hydrological processes. Hydrol. Earth Syst. Sci. 16:631–640. doi:10.5194/hess-16-631-2012

Goebel, M.-O., S.K. Woche, P.M. Abraham, G.E. Schaumann, and J. Bachmann. 2013. Water repellency enhances the deposition of negatively charged hydrophilic colloids in a water-saturated sand matrix. Colloids Surf. A 431:150–160. doi:10.1016/j.colsurfa.2013.04.038

Gonfiantini, R. 1986. Environmental isotopes in lake studies. In: P. Fritz and J. Ch. Fontes, editors, Handbook of environmental isotope geochemistry. Vol. 2. The terrestrial environment, B. Elsevier, Amsterdam. p. 113–168. doi:10.1016/B978-0-444-42225-5.50008-5

Good, S.P., D. Noone, and G. Bowen. 2015. Hydrologic connectivity constrains partitioning of global terrestrial water fluxes. Science 349:175–177. doi:10.1126/science.aaa5931

Gubiani, P.I., J.M. Reichert, C. Campbell, D.J. Reinert, and N.S. Gelain. 2013. Assessing errors and accuracy in dew-point potentiometer and pressure plate extractor measurements. Soil Sci. Soc. Am. J. 77:19–24. doi:10.2136/sssaj2012.0024

Hassan, M., S.K. Woche, and J. Bachmann. 2014. How the root zone modifies soil wettability: Model experiments with alfalfa and wheat. J. Plant Nutr. Soil Sci. 177:449–458. doi:10.1002/jpln.201300117

Hendry, M.J., E. Schmeling, L.I. Wassenaar, S.L. Barbour, and D. Pratt. 2015. Determining the stable isotope composition of pore water from saturated and unsaturated zone core: Improvements to the direct vapour equilibration laser spectrometry method. Hydrol. Earth Syst. Sci. 19:4427–4440. doi:10.5194/hess-19-4427-2015

Horita, J., K. Rozanski, and S. Cohen. 2008. Isotope effects in the evaporation of water: A status report of the Craig–Gordon model. Isot. Environ. Health Stud. 44:23–49. doi:10.1080/10256010801887174

Klaus, J., K.P. Chun, K.J. McGuire, and J.J. McDonnell. 2015. Temporal dynamics of catchment transit times from stable isotope data. Water Resour. Res. 51:4208–4223. doi:10.1002/2014WR016247

Koeniger, P., M. Gaj, M. Beyer, and T. Himmelsbach. 2016. Review on soil water isotope based groundwater recharge estimations. Hydrol. Processes 30:2817–2834. doi:10.1002/hyp.10775

Koeniger, P., J.D. Marshall, T. Link, and A. Mulch. 2011. An inexpensive, fast, and reliable method for vacuum extraction of soil and plant water for stable isotope analyses by mass spectrometry. Rapid Commun. Mass Spectrom. 25:3041–3048. doi:10.1002/rcm.5198

Lamparter, A., J. Bachmann, S.K. Woche, and M. Goebel. 2014. Biogeochemical interface formation: Wettability affected by organic matter sorption and microbial activity. Vadose Zone J. 13(7). doi:10.2136/vzj2013.10.0175

Lin, Y., and J. Horita. 2016. An experimental study on isotope fractionation in a mesoporous silica-water system with implications for vadose-zone hydrology. Geochim. Cosmochim. Acta 184:257–271. doi:10.1016/j.gca.2016.04.029

Lin, Y., J. Horita, and O. Abe. 2018. Adsorption isotope effects of water on mesoporous silica and alumina with implications for the land-vegetation-atmosphere system. Geochim. Cosmochim. Acta 223:520–536.

Liu, H., Z. Ju, J. Bachmann, R. Horton, and T. Ren. 2012. Moisture-dependent wettability of artificial hydrophobic soils and its relevance for soil water desorption curves. Soil Sci. Soc. Am. J. 76:342–349. doi:10.2136/sssaj2011.0081

Majoube, M. 1971. Fractionemente oxygene 18 entre la glace et la vapeurd'eau. J. Chim. Phys. 68:625–636. doi:10.1051/jcp/1971680625

McDonnell, J.J. 2014. The two water worlds hypothesis: Ecohydrological separation of water between streams and trees? Wiley Interdiscip. Rev.: Water 1:323–329. doi:10.1002/wat2.1027

McGuire, K.J., and J.J. McDonnell. 2006. A review and evaluation of catchment transit time modeling. J. Hydrol. 330(3-4):543–563. doi:10.1016/j.jhydrol.2006.04.020

Meißner, M., M. Köhler, L. Schwendenmann, D. Hölscher, and J. Dyckmans. 2014. Soil water uptake by trees using water stable isotopes (δ^2H and δ^{18}O): A method test regarding soil moisture, texture and carbonate. Plant Soil 376:327–335.

Müehl, G.J.H., J. Rüehlmann, M.O. Goebel, and J. Bachmann. 2012. Application of confocal laser scanning microscopy (CLSM) to visualize the effect of porous media wettability on unsaturated pore water configuration. J. Soils Sediments 12:75–85. doi:10.1007/s11368-011-0395-7

Mueller, M.H., A. Alaoui, C. Kuells, H. Leistert, K. Meusburger, and C. Stumpp. 2014. Tracking water pathways in steep hillslopes by δ^{18}O depth profiles of soil water. J. Hydrol. 519:340–352. doi:10.1016/j.jhydrol.2014.07.031

Oerter, E.J., and G. Bowen. 2017. In situ monitoring of H and O stable isotopes in soil water reveals ecohydrologic dynamics in managed soil systems. Ecohydrology 10:e1841. doi:10.1002/eco.1841

Oerter, E., K. Finstad, J. Schaefer, G.R. Goldsmith, T. Dawson, and R. Amundson. 2014. Oxygen isotope fractionation effects in soil water via interaction with cations (Mg, Ca, K, Na) adsorbed to phyllosilicate clay minerals. J. Hydrol. 515:1–9. doi:10.1016/j.jhydrol.2014.04.029

Orlowski, N., D.L. Pratt, and J.J. McDonnell. 2016. Intercomparison of soil pore water extraction methods for stable isotope analysis. Hydrol. Processes 30:3434–3449. doi:10.1002/hyp.10870

Oshun, J., W.E. Dietrich, T.E. Dawson, and I. Fung. 2016. Dynamic, structured heterogeneity of water isotopes inside hillslopes. Water Resour. Res. 52:164–189. doi:10.1002/2015WR017485

Othmer H., B. Diekkrüger, and M. Kutilek. 1991. Bimodal porosity and unsaturated hydraulic conductivity. Soil Sci. 152:139–150.

Peters, A., C.I. Sascha, and W. Durner. 2015. Revisiting the simplified evaporation method: Identification of hydraulic functions considering vapor, film and corner flow. J. Hydrol. 527:531–542. doi:10.1016/j.jhydrol.2015.05.020

Pronk, G.J., K. Heister, C. Vogel, D. Babin, J. Bachmann, G.-C. Ding, et al. 2017. Interaction of minerals, organic matter, and microorganisms during biogeochemical interface formation as shown by a series of artificial soil experiments. Biol. Fertil. Soils 53:9–22. doi:10.1007/s00374-016-1161-1

Reszkowska, A., J. Bachmann, A. Lamparter, E. Diamantopoulos, and W. Durner. 2014. The effect of temperature-induced soil water repellency on transient capillary pressure–water content relations during capillary rise. Eur. J. Soil Sci. 65:369–376.

Rothfuss, Y., I. Braud, N. Le Moine, P. Biron, J.-L. Durand, M. Vauclin, and T. Bariac. 2012. Factors controlling the isotopic partitioning between soil evaporation and plant transpiration: Assessment using a multi-objective calibration of SiSPAT-Isotope under controlled conditions. J. Hydrol. 442-443:75–88. doi:10.1016/j.jhydrol.2012.03.041

Rothfuss, Y., and M. Javaux. 2017. Reviews and syntheses: Isotopic approaches to quantify root water uptake: A review and comparison of methods. Biogeosciences 14:2199–2224. doi:10.5194/bg-14-2199-2017

Rothfuss, Y., S. Merz, J. Vanderborght, N. Hermes, A. Weuthen, A. Pohlmeier, H. Vereecken, and N. Brüggemann. 2015. Long-term and high-frequency non-destructive monitoring of water stable isotope profiles in an evaporating soil column. Hydrol. Earth Syst. Sci. 19:4067–4080. doi:10.5194/hess-19-4067-2015

Rothfuss, Y., H. Vereecken, and N. Brüggemann. 2013. Monitoring water stable isotopic composition in soils using gas-permeable tubing and infrared laser absorption spectroscopy. Water Resour. Res. 49:3747–3755. doi:10.1002/wrcr.20311

Skrzypek, G., A. Mydłowski, S. Dogramaci, P. Hedley, J.J. Gibson, and P.F. Grierson. 2015. Estimation of evaporative loss based on the stable isotope composition of water using *Hydrocalculator*. J. Hydrol. 523:781–789. doi:10.1016/j.jhydrol.2015.02.010

Soderberg, K., S.P. Good, L. Wang, and K. Caylor. 2012. Stable isotopes of water vapor in the vadose zone: A review of measurement and modeling techniques. Vadose Zone J. 11(3). doi:10.2136/vzj2011.0165

Sprenger, M., B. Herbstritt, and M. Weiler. 2015. Established methods and new opportunities for pore water stable isotope analysis. Hydrol. Processes 29:5174–5192. doi:10.1002/hyp.10643

Sprenger, M., H. Leistert, K. Gimbel, and M. Weiler. 2016. Illuminating hydrological processes at the soil–vegetation–atmosphere interface with water stable isotopes. Rev. Geophys. 54:674–704. doi:10.1002/2015RG000515

Stumpp, C., and P. Maloszewski. 2010. Quantification of preferential flow and flow heterogeneities in an unsaturated soil planted with different crops using the environmental isotope δ^{18}O. J. Hydrol. 394:407–415. doi:10.1016/j.jhydrol.2010.09.014

van Genuchten, M.Th. 1980. A closed-form equation for predicting the hydraulic conductivity of unsaturated soils. Soil Sci. Soc. Am. J. 44:892–898. doi:10.2136/sssaj1980.03615995004400050002x

Vargas, A.I., B. Schaffer, L. Yuhong, and L.S.L. Sternberg. 2017. Testing plant use of mobile vs immobile soil water sources using stable isotope experiments. New Phytol. 215:582–594.

Vereecken, H., A. Schnepf, J.W. Hopmans, M. Javaux, D. Or, and T. Roose. 2016. Modeling soil processes: Review, key challenges, and new perspectives. Vadose Zone J. 15(5). doi:10.2136/vzj2015.09.0131

Volkmann, T., and M. Weiler. 2014. Continual in-situ monitoring of pore water stable isotopes. Hydrol. Earth Syst. Sci. 18:1819–1833. doi:10.5194/hess-18-1819-2014

Wassenaar, L.I., M.J. Hendry, V.L. Chostner, and G.P. Lis. 2008. High resolution pore water ^{2}H and ^{18}O measurements by $H_2O_{[liquid]}$–$H_2O_{[vapor]}$ equilibration laser spectroscopy. Environ. Sci. Technol. 42:9262–9267. doi:10.1021/es802065s

West, A.G., S.J. Patrickson, and J.R. Ehleringer. 2006. Water extraction times for plant and soil materials used in stable isotope analysis. Rapid Commun. Mass Spectrom. 20:1317–1321.

Woche, S.K., M. Goebel, R. Mikutta, C. Schurig, M. Kaestner, G. Guggenberger, and J. Bachmann. 2017. Soil wettability can be explained by the chemical composition of particle interfaces: An XPS study. Sci. Rep. 7:42877. doi:10.1038/srep42877